Available online at www.sciencedirect.com
ScienceDirect
Journal of the European Ceramic Society 30 (2010) 1027–1034
www.elsevier.com/locate/jeurceramsoc

Characterization of pop-in phenomena and indentation modulus in a polycrystalline ZrB_2 ceramic

Stefano Guicciardi *, Cesare Melandri, Frederic Tullio Monteverde

ISTEC-CNR, Via Granarolo 64, I-48018 Faenza (RA), Italy

Received 13 May 2009; received in revised form 2 October 2009; accepted 20 October 2009
Available online 20 November 2009

Abstract

Low-load nanoindentation tests were carried out on a polycrystalline ZrB_2-based ceramic. Pop-in phenomena were observed when indentation marks were placed in the interior of the ZrB_2 grains. Both pop-in loads and pop-in extents were statistically distributed with a mutual strong correlation. The critical shear stresses at pop-in were in good agreement with the theoretical shear strength of ZrB_2. The experimental pop-in extents were also compared to a simplified model developed for homogeneous dislocation nucleation. The influence of the grain orientation on the indentation modulus was derived from the model of Delafargue and Ulm (2004)[50] and compared to the experimental results. Some results were definitely influenced by the polycrystalline structure of the investigated ceramic.

Keywords: Mechanical properties; Plasticity; Nanoindentation; Borides

1. Introduction

Zirconium diboride (ZrB_2) is a refractory ceramic belonging to the Ultra High Temperature Ceramics (UHTC) family currently under study for aerospace applications.[1,2] To the authors' knowledge only one paper has been published on the nanoindentation behaviour of this material.[3] Nanoindentation tests are of paramount importance in order to characterize the mechanical behaviour of a material on a very small scale when only tiny portions of volume are stresses as it is the case in applications involving wear or contact. During a series of low-load nanoindentation tests on a ZrB_2 ceramic we have recently observed that the load–displacement curves displayed a sudden pop-in at the beginning of loading. This kind of phenomenon has been noted in metals,[4–7] semi-conductors[8–10] and ceramics.[11–16] Many studies have reported that before the pop-in the unloading curve would superimpose to the loading curve indicating that till that point no dissipative mechanisms, i.e. plasticity, took place. After the pop-in, instead, hysteresis in the loading–unloading cycle appeared. In an aluminium film, *in situ* TEM analysis has clearly shown the appearance of dislocations in correspondence of the pop-in.[17] The most widely accepted explanation of pop-in is homogeneous dislocation nucleation.[18] This is also supported by atomistic simulations of indentation in perfect crystals.[19,20] There are however some experimental and theoretical evidences that this event can be triggered by heterogeneous dislocation nucleation when the material surface presents surface steps or ledges.[21,22] Other experimental results seem instead to indicate a stress-rate dependent mechanisms. For a 4H SiC, a direct relationship was found between the stress-rate and the pop-in load[23,24] but the opposite was observed on specific crystallographic planes for sapphire.[25] However, experimental results have been presented in which the load at pop-in was shown to be independent on the loading rate in several metals and semi-conductors.[9,26] Finally, non-dislocation driven explanations were recently proposed for pop-in phenomena such as phase transformation in GaAs[27,28] and twinning in sapphire.[25,29] One of the main support to the theory of homogeneous dislocation nucleation is that the shear stress at which pop-in occurs is usually in very good agreement with the theoretical shear strength of the indented material. Though the form in which engineering materials are most often employed is polycrystalline, the main part of studies on incipient plasticity was focused on monocrystals to avoid

* Corresponding author. Tel.: +39 0546 699720; fax: +39 0546 46381.
E-mail address: stefano.guicciardi@istec.cnr.it (S. Guicciardi).

0955-2219/$ – see front matter © 2009 Elsevier Ltd. All rights reserved.
doi:10.1016/j.jeurceramsoc.2009.10.014

the complications deriving from grain size and grain boundaries.

In this study, pop-in phenomena in a polycrystalline ZrB_2 ceramic are presented and discussed. It will be shown that the experimental findings can support the theory of homogeneous dislocation nucleation. Moreover, the indentation modulus will be compared to bounds related to the different grains orientation.

2. Experimental

Starting from commercial ZrB_2 (grade B, H.C. Starck, Germany) and SiC (grade UF25, H.C. Starck, Germany) powders, a mixture of ZrB_2 + 5 vol.% SiC was prepared. This mixture was then sintered in fully dense form by hot-pressing at 1900 °C for 25 min with a maximum applied pressure of 50 MPa. Final density and mean grain size were 5.96 g/cm^3 and 4.5 μm, respectively. From the sintered pellet, a sample was cut and machined. This sample was subsequently resin-mounted and polished down to 0.25 μm with diamond-based pastes. The last polishing step was performed with colloidal silica. The final mean surface roughness, R_a, was (31 ± 2) nm, as measured with a contact-stylus profilometer (Talysurf Plus, Rank Taylor, UK). The polished sample was then removed from the resin block and glued to an aluminum cylinder for the nanoindentation tests which were carried out on a commercial MTS nanoindenter mod. XP (MTS, Oak Ridge, USA) fitted with a berkovich indenter. The loading–unloading cycle consisted in a loading ramp up to 5 mN in 10 s, no holding time and an unloading ramp with the same speed as the loading one. The peak load was chosen so that the indentation mark could be well-confined inside single grains but with a maximum penetration depth sufficiently high to be interpreted using the area function for a berkovich indenter. The indenter tip geometry was properly calibrated on a standard fused silica sample as explained later. Hardness and indentation modulus were calculated on the basis of the Oliver ad Pharr (OP) model[30] by the software TestWork ver. 4.06a. This software automatically subtracts the machine compliance and the thermal drift from the raw data. The indentations, a total of 123, were organized in a matrix form (41 × 3) with a vertical and horizontal distance of 2 μm between each indent. The indents grid was observed under SEM (Cambridge S360, Cambridge, U.K.). Some indents were also scanned by AFM (Scanning Probe Microscope Vista-100, Burleigh Instruments Inc., USA).

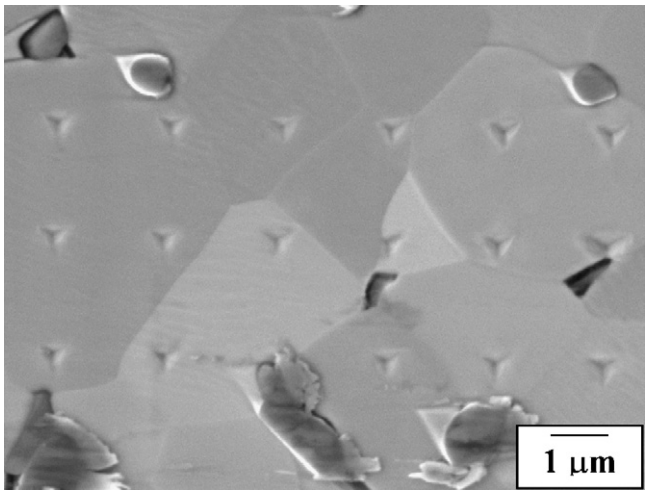

Fig. 2. SEM micrograph of a selected area of the indentation grid. The dark gray particles are SiC while the matrix is ZrB_2. Some ZrB_2 grains can be easily distinguished due to their different orientation.

3. Results and discussion

3.1. Pop-in analysis

Two typical examples of loading–unloading cycle in the investigated material are shown in Fig. 1. As can be seen, in the first case an evident pop-in occurred at about 2.6 mN, Fig. 1a. In the second case, such a pop-in was not observed, Fig. 1b. With the aid of the indentation grid map, an example of which is shown in Fig. 2, it was possible to establish a correspondence between the loading–unloading curves and the indentation marks. It was thus observed that the loading–unloading cycle shown in Fig. 1b were in correspondence of indentation marks placed into the SiC phase, SiC/ZrB_2 or ZrB_2/ZrB_2 boundaries. When the indentation marks were clearly placed into the interior of the ZrB_2 grains, the majority of the loading–unloading cycles was mainly of the type shown in Fig. 1a. Out of 90 indentations into the interior of ZrB_2 grains, 88 were of the type shown in Fig. 1a and only two were of the type shown

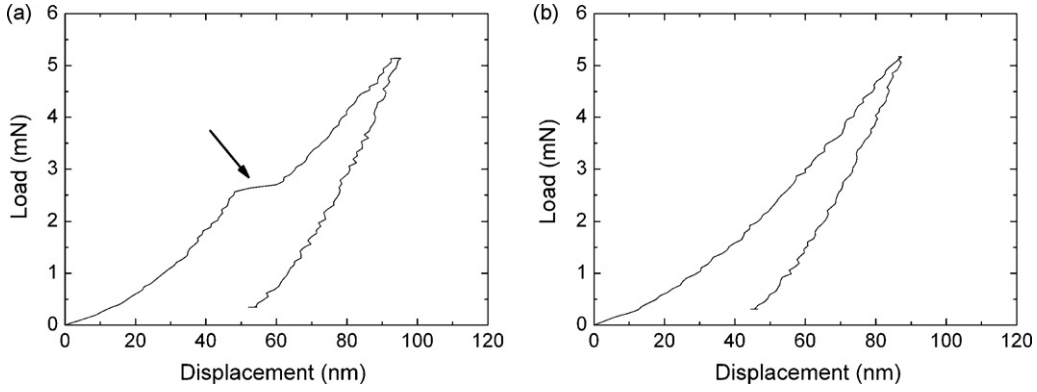

Fig. 1. Examples of loading–unloading curves in the ZrB_2–5 vol.% SiC material and (a) loading curve with pop-in indicated by the arrow and (b) smooth curve.

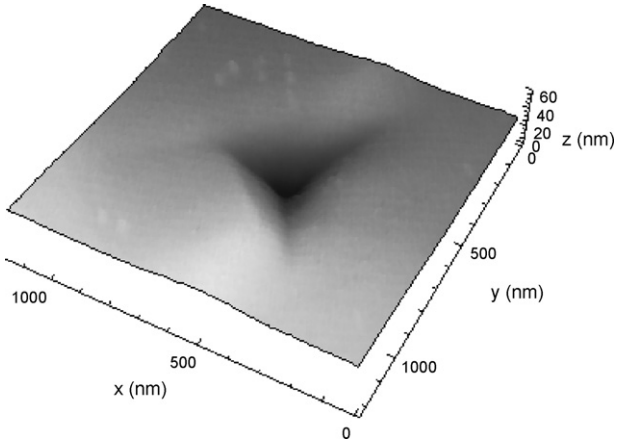

Fig. 3. AFM image of a 5-mN indent in a ZrB_2 grain which exhibited pop-in. No evidence of microcrack can be observed.

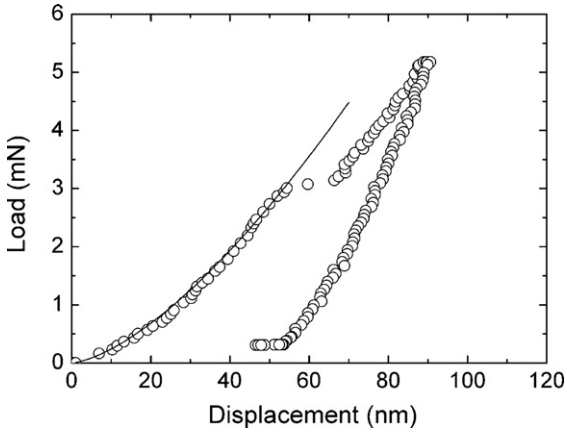

Fig. 4. Comparison between the loading–unloading cycle (empty circles) with Hertz theory (continuous line). Note the very good agreement up to the pop-in.

in Fig. 1b. These latter curves were placed into the interior of two different grains. At first sight, it could be surprising that a polished surface as that of our sample exhibits pop-in phenomena as these are usually observed only in flat monocrystals or chemically polished surfaces. The mechanical polishing procedure is in fact thought to introduce a high dislocation density at the surface so that during loading a smooth transition between the elastic and plastic behaviour occurs.[31] However, the appearance of pop-in was previously observed also in other ceramics whose surface was prepared by mechanical polishing.[14,32]

The rationale of the detected pop-in excursions will be in the following presented at the light of dislocation activity. The occurrence of pop-in due to an eventual phase transformation cannot be of course excluded but at the moment it is out of our investigation capabilities. The stress-rate dependence of pop-in is instead demanded to a future work. As can be seen in Fig. 3, the AFM inspection of some indents characterized by pop-in excluded the presence of microcracks or linear surface features (LSF) such those observed around indentations in sapphire which are the effects of twinning.[25,29,33] When some indentation tests were carried out in the ZrB_2 phase at a peak load of 1 mN in most cases no hysteresis in the loading–unloading cycles was observed indicating a totally elastic behaviour. To further support the fact that the observed pop-in is very likely due to dislocation activity, a comparison of the experimental loading curves with the elastic Hertz theory was carried out. In order to make use of the Hertz theory, the geometry of the tip indenter for small penetrations, i.e. the tip radius R, had to be evaluated. This was accomplished by performing 10 μN load tests on a standard fused silica specimen. In these fully elastic tests, the load P is related to the displacement h through the reduced Young's modulus E^* as follows[34]:

$$P = \frac{4}{3}E^*\sqrt{R}h^{3/2} \tag{1}$$

where the reduced Young's modulus E^* is given by the combination of the elastic constants of the tested material, E_m and ν_m, and tip material, E_i and ν_i,

$$\frac{1}{E^*} = \frac{1-\nu_m^2}{E_m} + \frac{1-\nu_i^2}{E_i} \tag{2}$$

For silica and diamond, Young's modulus and Poisson ratio were taken as 72 and 1141 GPa, and 0.17 and 0.07, respectively. The tip radius estimate was (221 ± 54) nm as averaged on ten tests. In Fig. 4, it is shown an example of the comparison between a loading–unloading cycle which was characterized by the presence of pop-in and Eq. (1). In this case, the reduced Young's modulus was the combination of the diamond elastic constants and those of ZrB_2. The ZrB_2 indentation modulus was calculated on the unloading curve according to the OP model, while for the Poisson ratio a value of 0.11 was considered.[35] As can be seen, the match between the loading curve before pop-in and Hertz theory is very good confirming that the pop-in events marked the departure from a fully elastic to an elasto-plastic behaviour.

Hertz theory can be further exploited to compare the shear stress at pop-in with the theoretical shear strength of ZrB_2. According to the previous tip radius estimation, the indenter tip can be assumed to behave like a spherical-tip up to a maximum contact depth h_s of 29 nm,[36] see Fig. 5. The apex angle α was calculated from the first constant of our berkovich area function and resulted to be 69.2°. To properly calculate the shear

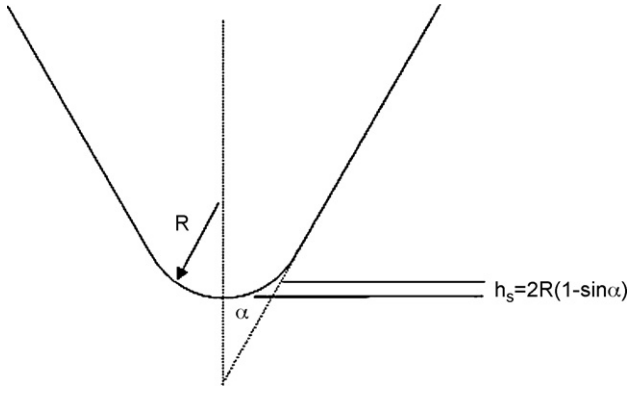

Fig. 5. Idealized geometry of the berkovich indenter tip. See text for the definition of the symbols.

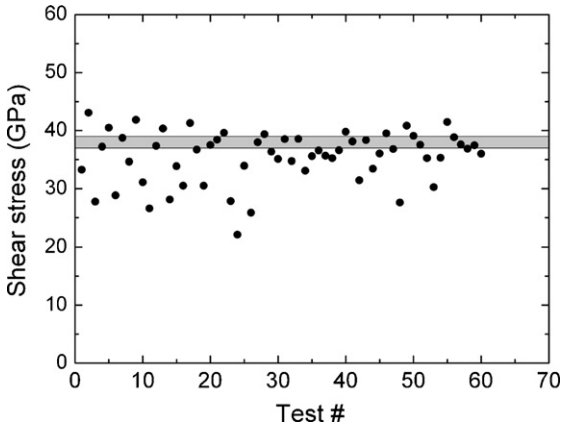

Fig. 6. Experimental shear stress vs. test no. The gray region represents the area between the lower and upper limit of ZrB_2 theoretical shear strength.

stresses according to Hertz theory, in the following only tests whose elastic part of the loading curve, i.e. that before pop-in, was less than 58 nm will be considered. This comes from the fact that in an elastic contact the contact depth is half the total penetration.[34] For total penetrations deeper than 58 nm, the contact geometry cannot be longer considered that of a sphere into a half-space and this complicates the governing formulas.[37] In an elastic contact, a load P on a spherical-tip pressed into a flat surface generates a shear stress whose maximum value is,[38]

$$\tau_{\max} = 0.31 p_0 \tag{3}$$

where

$$p_0 = \left(\frac{6PE^*}{\pi^3 R^2}\right)^{1/3} \tag{4}$$

with the usual meaning of the symbols. Therefore, considering the loads in correspondence of the pop-in excursions, the maximum shear stress can be calculated and compared with the theoretical value of ZrB_2 shear strength which is given by $G/2\pi$.[39] Since ZrB_2 is an hexagonal crystal, two engineering shear moduli have to be considered, the shear modulus parallel to the hexagonal axis, which is given by C_{44}, and that one perpendicular to the hexagonal axis, which is given by $(1/2)(C_{11} - C_{12})$.[40] For ZrB_2, the following elastic constants were considered, $C_{11} = C_{22} = 567.8$ GPa, $C_{12} = 56.9$ GPa, $C_{44} = 247.5$ GPa, $C_{33} = 436.1$ GPa and $C_{13} = 120.5$ GPa.[41] From these values, the theoretical shear strength in the two perpendicular directions resulted to be about 39 and 41 GPa, respectively. These values are shown as horizontal lines in Fig. 6 where they are compared with the experimental values of shear stress calculated at pop-in. As can be seen, there is a good agreement between the theoretical and the experimental values even though a part of the experimental points fall just below these two limits. This was very likely due to the presence of surface defects in our specimen as steps or roughness which can lower the yield point at which pop-in occurs.[42] Moreover, it has been shown that at low penetration depths a spherical-tip assumption for a berkovich tip could underestimate of about 17% the real shear stress due to tip imperfections.[43]

The above analysis was based on linear elasticity, as it is usually found in most of the literature. However, it should be kept present that *ab initio* calculations indicate an evident non-linearity in the stress–strain curve close to the yield point.[44] Ignoring this non-linearity can overestimate the experimental shear strength in a way that depends on the indentation strain. From Fig. 3b of Ref. 44 we could estimate an overestimation of our experimental results of about 8%. All the above considered, the agreement between the experimental shear strengths and the theoretical expectations can be considered satisfactorily.

The pop-in absence when an indentation was placed across a ZrB_2/ZrB_2 grain boundary rules out that the mechanism responsible of the observed pop-in was a dislocations burst across grain boundaries[45] as well as the attainment of a critical condition, i.e. the availability of mobile dislocations.[46]

To further test the hypothesis that pop-in was due to homogeneous dislocation nucleation, a comparison between the observed and the expected pop-in extents was attempted using the theory presented by Gouldstone et al.[6] According to this theory, the pop-in extents can be estimated by considering an overall energy balance between the elastic energy, the dislocations interaction energy and the dislocations self-energy,

$$W_e = W_i^t + W_s^t \tag{5}$$

where W_e is the total elastic energy which can be calculated as the area under the loading curve up to the pop-in

$$W_e = \int_0^{h_p} \frac{4}{3} PE^* \sqrt{R} x^{3/2} dx \tag{6}$$

where h_p is the displacement at pop-in and all the other symbols have the usual meaning. By invoking some simplifying assumptions, Gouldstone et al.[6] expressed the interaction energy of the dislocation loops created by the indentation, W_i^t, as,

$$W_i^t = \frac{Gb^2}{1-\nu} R_d \left\{ \sum_{j=1}^{N-1} j \left(\ln \frac{8R_d}{\rho} \right) - \sum_{j=1}^{N-1} \ln(j!) - \sum_{j=1}^{N-1} j \right\} \tag{7}$$

where G is the shear modulus, b is the burger vector, 0.3 nm for ZrB_2,[35] R_d is the dislocation loop radius at pop-in and ρ is the dislocation loop spacing. In the original paper, which dealt with thin films, ρ was calculated as t_f/N where t_f was the film thickness[6] and N the total number of dislocation loops created at pop-in. In our case, for t_f we considered half the mean grain size. The total self-energy term W_s^t was given as

$$W_s^t = N \frac{Gb^2}{2(1-\nu)} R_d \left(\ln \frac{8R_d}{\rho} - 1 \right) \tag{8}$$

Differently from Gouldstone et al.,[6] who estimated the dislocation loop radius ρ introducing a numerical value for N and compared that estimate to the indentation contact radius at pop-in a, we used a commercial mathematical software (MATHEMATICA 6, Wolfram Research Inc., IL, USA) to calculate N, and hence the pop-in extent Nb, by inserting the known inden-

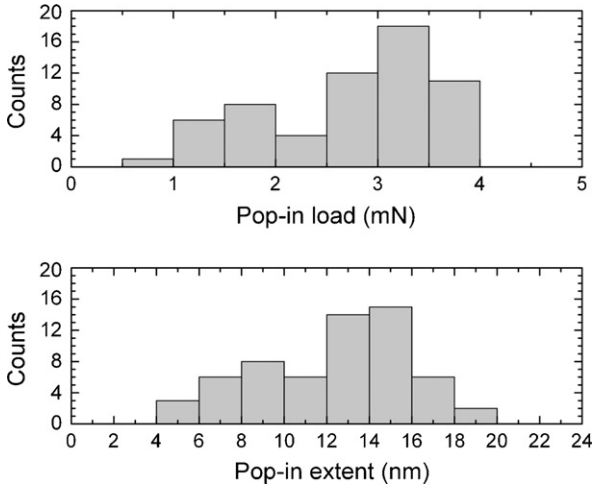

Fig. 7. Histograms of pop-in load (above) and pop-in extent (below). Note the almost bi-modal distribution in both group of data.

tation contact radius a, given by,[38]

$$a = \left(\frac{3PR}{4E^*}\right)^{1/3} \quad (9)$$

in place of the dislocation loop radius ρ in Eqs. (7) and (8). For G, the average between the value along the hexagonal axis and that perpendicular to the hexagonal axis was used, 251 GPa. The expected pop-in extent calculated according to the above theory turned out to be an almost constant value of about 20 nm, which has to be compared to the experimental average pop-in extent of 11.8 nm. Considering all the simplifying assumptions implicated in the model and the presence of surface defects which lower the shear stress at pop-in, the agreement can be considered good. This strengthens the hypothesis that the observed pop-in excursions were due to homogeneous dislocation nucleation.

3.2. Influence of microstructure on pop-in

Both pop-in loads and pop-in extents showed a bi-modal statistical distribution, Fig. 7. Besides the different grain orientation, the scatter in pop-in load and pop-in extent could also be due to surface defects,[7] grain boundary proximity[32] and grain size.[47] Even though the employed analytical techniques did not allow to determine the orientation of the ZrB_2 grains included

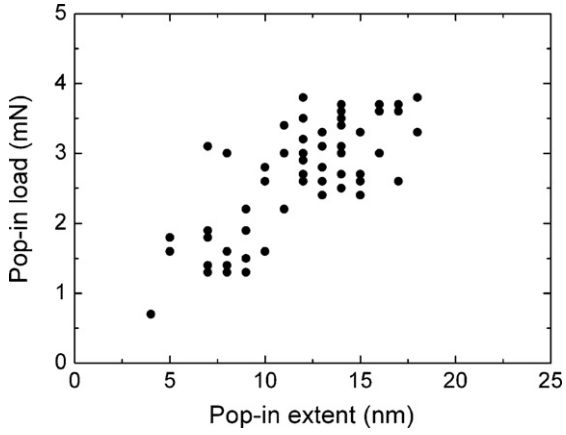

Fig. 8. Pop-in load vs. pop-in extent. As can be seen, the pop-in load clearly increases with the increasing of the pop-in extent.

in the indentation grid, we found a strong correlation between pop-in loads and pop-in extents, see Fig. 8, as reported by several authors in other materials.[10,48,49]

Due to the small grain size of the ZrB_2 matrix, not many indents could be placed inside a single grain. When this was the case, both pop-in loads and pop-in extents were similar, Fig. 9a. The same was observed in a ZrO_2 ceramic material.[32] However, when an indent was placed very close to a grain boundary, both pop-in load and pop-in extent decreased, Fig. 9b, as it was reported for a gold film.[7]

3.3. Comparison with expected indentation modulus

In this section, we will consider all the indentation modulus values of the ZrB_2 phase as calculated by the OP model from the unloading curve of the nanoindentation tests, without any regard to the presence, or not, of the pop-in phenomenon. According to the traditional OP analysis, hardness, which will not be discussed here, and indentation modulus of the ZrB_2 phase were (32.2 ± 3.0) and (563 ± 57) GPa, respectively. For these calculations, the berkovich area function was previously calibrated on a standard fused silica specimen and checked before and after the nanoindentation tests. For penetration depths comparable to those recorded in the ZrB_2 phase, we observed a difference between the silica reference Young's modulus value of 72 GPa and the silica experimental indentation modulus of about 1%,

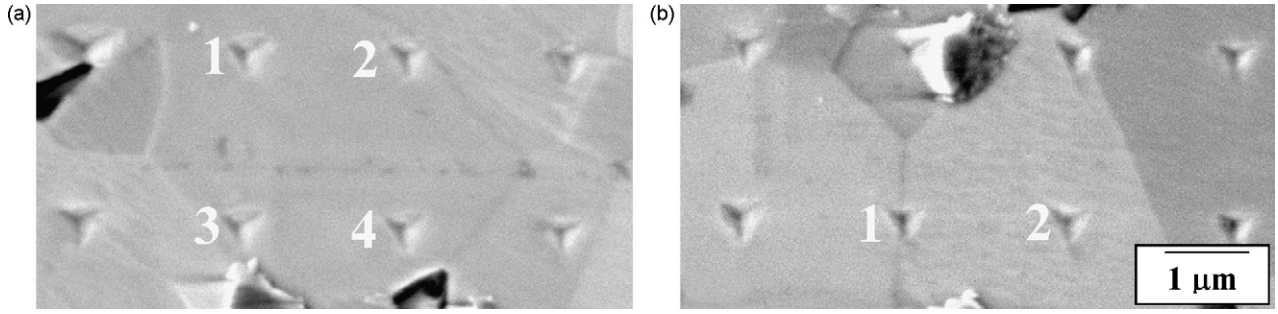

Fig. 9. (a) Four indents placed inside a single grain. Pop-in load and pop-in extent were the following: (1) 3.0 mN, 8 nm; (2) 3.4 mN, 11 nm; (3) 3.5 mN, 12 nm; (4) 3.0 mN, 11 nm and (b) two indents inside a single grain but with indent 1 almost across a ZrB_2/ZrB_2 grain boundary. Pop-in load and pop-in extent of indent 1 were 1.9 mN and 7 nm, respectively. For indent 2, 2.6 mN and 17 nm.

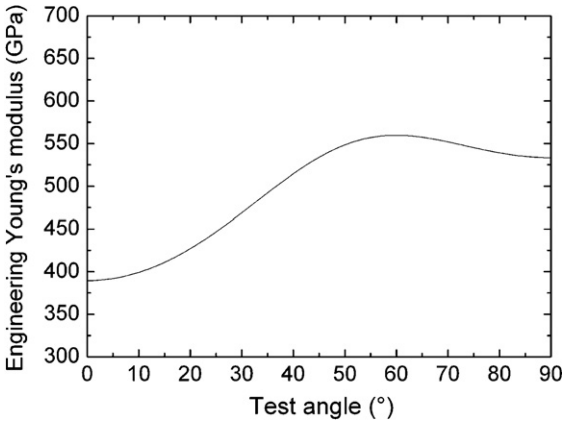

Fig. 10. Engineering Young's modulus as a function of the angle between the testing direction and the hexagonal axis of the ZrB_2 monocrystal.

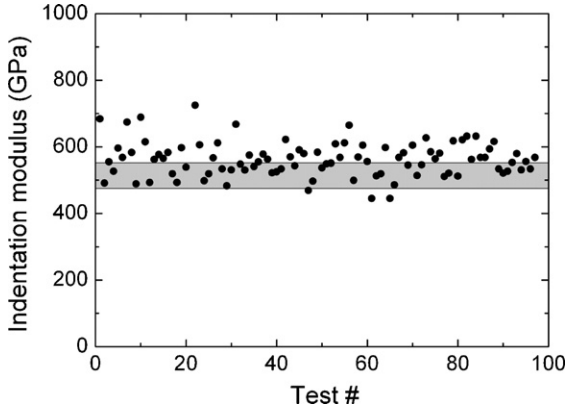

Fig. 11. Indentation modulus vs. test no. The gray region represents the area between the lower and upper limit as calculated from the elastic constant of the ZrB_2 hexagonal crystal.

which can be taken as a rough estimate of the measurement precision.

As can be seen in Fig. 2, most of the indentation marks were well-confined inside single grains. The indentation modulus values were therefore definitely influenced by the different orientations of the grains even if some effects of the surrounding grains cannot be disregarded due to the long range of the elastic field of an indentation.[38] Just to give an indication of the influence of the ZrB_2 crystal orientation on the Young's modulus measurement, Fig. 10 shows the variation of the engineering Young's modulus of a ZrB_2 monocrystal with the angle θ that the testing direction makes with respect to the axis of symmetry which is perpendicular to the basal plane.[41] This is the situation where the maximum variation is observed as ZrB_2 is a transversely isotropic solid. As can be seen, the lowest value, 390 GPa, is found when ZrB_2 is tested along the axis of symmetry ($\theta = 0^\circ$), the highest value, 560 GPa, is found when the testing angle is about 60°. In direction perpendicular to the basal plane ($\theta = 90^\circ$), the engineering Young's modulus is 533 GPa. Due to the three-dimensional stress field below the indenter, however, the indentation modulus of a single crystal is a different combination of the single crystals elastic constants with respect to the engineering Young's modulus. Some models have been proposed in order to estimate the indentation modulus according to the different orientation of an indented crystal as a function of its elastic constants. Here, we compare our experimental results to the model proposed by Delafargue and Ulm[50] which is simpler than the model proposed by Vlassak and Nix.[51] The former model provides formulas to easily estimate the indentation modulus M (in this section we will use the same notation of those authors) of a transversely isotropic medium when indented by a conical indenter along the axis of symmetry and perpendicularly to it. M represents the reduced indentation modulus, i.e. the combination of the indentation modulus and Poisson ratio of the material (m) and indenter (i),

$$\frac{1}{M} = \frac{1-\nu_m^2}{M_m} + \frac{1-\nu_i^2}{M_i} \tag{10}$$

The equations to obtain the indentation modulus in the axis of symmetry, M_3 in their notation, and the indentation modulus in the plane perpendicular to this, M_1, are,

$$M_3 = 2\sqrt{\frac{C_{31}^2 - C_{13}^2}{C_{11}}\left(\frac{1}{C_{44}} + \frac{2}{C_{31}+C_{13}}\right)^{-1}} \tag{11}$$

$$M_1 = \sqrt{M_{12}M_{13}} \tag{12}$$

where $C_{31} = \sqrt{C_{11}C_{33}} > C_{13}$, $M_{12} = \sqrt{(C_{11}/C_{33})}M_3$ and $M_{13} = (C_{11}^2 - C_{12}^2/C_{11})$. The ZrB_2 elastic constants to be introduced in the above equations have been presented in Section 1. The calculated values of M_3 and M_1 were 475 and 552 GPa, respectively. Fig. 11 shows the comparison of our experimental values with these limiting values. Just for comparison purposes, the Hashin–Shtrikman lower and upper bounds of the engineering Young's modulus calculated according to Ref. 52 with the elastic constant reported in Section 2 are 521 and 532 GPa, respectively. As can be seen from Fig. 11, many experimental points fall inside the indentation modulus limits, however a large number of points fall outside, mainly above the upper value, with differences which were higher than the measurement precision. This was unexpected as microstructural effects coming from neighbouring grains, material defects, grain boundaries or triple points should have lowered the experimental values and not vice versa. A possible partial explanation is that the highest value of ZrB_2 Young's modulus is in a direction which is not perpendicular to the axis of symmetry but at an angle of about 60°, see Fig. 10, so that the upper limit in Fig. 11 should be located higher than the actual position, of about 4% if the ratio between the values of Fig. 10 hold true. Another possible explanation is that we are comparing data obtained with indentation tests with limits calculated from elastic constants measured by resonance.[41] It is in fact known that indentation tends to overestimated the Young's modulus of a material with respect to other techniques.[53–55] As it was for our case, for example, also some experimental values by Hay et al.[56] on β-Si_3N_4 grains are above the upper limit of the indentation modulus which can be calculated starting from the β-Si_3N_4 elastic constants measured by Brillouin scattering and reported in Ref. 57.

4. Conclusions

Nanoindentation tests with a peak load of 5 mN were carried out on a polycrystalline ZrB_2–5 vol.% SiC ceramic composite. When the indentations were placed in the interior of the ZrB_2 grains, pop-in excursion occurred most of the times. Pop-in was not observed when the indents were placed in the SiC phase, ZrB_2/SiC boundary or ZrB_2/ZrB_2 grain boundary. Besides the experimental evidence that no microcracks or linear surface features were observed around the indents, a comparison with Hertz theory showed that pop-in could be due to dislocation activity. Also the critical shear stresses at pop-in were in good agreement with the theoretical shear strength of ZrB_2. Pop-in loads and pop-in extents were strongly correlated and both exhibited a bimodal statistical distribution. The fair agreement found between the experimental pop-in extents and the pop-in extents estimated by a simplified model further supports the conjecture that pop-in in this ceramic material is due to homogeneous dislocation nucleation. The experimental values of Young's modulus were compared with the indentation modulus prediction of Delafargue and Ulm[50]. While many experimental values were in good agreement with the expected limits, part of the data was well above the upper limit.

Note added in proof

It has come to the attention of the authors a recently published paper on the room-temperature dislocation activity in ZrB2 polycrystalline ceramic which indicates that in this ceramic dislocation slip occurs on multiple intersecting slip bands [Ghosh D, Subhash G, Bourne GR. Room-temperature dislocation activity during mechanical deformation in polycrystalline ultra-high-temperature ceramics, *Scripta Materialia* **61** (2009) 1075–8]. This strengthens our hypothesis that pop-in was due to homogeneous dislocation nucleation.

Acknowledgments

The authors would like to thank Prof. C. Martini and Dr. L. Micele (SMETEC, University of Bologna) for the AFM analysis. The authors would also thank the referee for the very useful suggestions.

References

1. Opeka MM, Talmy IG, Wuchina EJ, Zaykoski JA, Causey SJ. Mechanical, thermal, and oxidation properties of refractory hafnium and zirconium compounds. *Journal of the European Ceramic Society* 1999;**19**: 2405–14.
2. Levine SR, Opila EJ, Halbig MC, Kiser JD, Singh M, Salem JA. Evaluation of ultra-high temperature ceramics for aeropropulsion use. *Journal of the European Ceramic Society* 2002;**22**:2757–67.
3. Guicciardi S, Melandri C, Silvestroni L, Sciti D. Indentation grid analysis of nanoindentation bulk and in situ properties of ceramic phases. *Journal of Materials Science* 2008;**43**:4348–52.
4. Gerberich WW, Nelson JC, Lilleodden ET, Anderson P, Wyrobek JT. Indentation induced dislocation nucleation: the initial yield point. *Acta Materialia* 1996;**44**:3585–98.
5. Michalske TA, Houston JE. Dislocation nucleation at nano-scale mechanical contacts. *Acta Materialia* 1998;**46**:391–6.
6. Gouldstone A, Koh HJ, Zeng KY, Giannakopoulos AE, Suresh S. Discrete and continuous deformation during nanoindentation of thin films. *Acta Materialia* 2000;**48**:2277–95.
7. Lilleodden ET, Nix WD. Microstructural length-scale effects in the nanoindentation behavior of thin gold films. *Acta Materialia* 2006;**54**: 1583–93.
8. Mann AB, Pethica JB. The effect of tip momentum on the contact stiffness and yielding during nanoindentation testing. *Philosophical Magazine A-Physics of Condensed Matter Structure Defects and Mechanical Properties* 1999;**79**:577–92.
9. Lorenz D, Zeckzer A, Hilpert U, Grau P, Johansen H, Leipner HS. Pop-in effect as homogeneous nucleation of dislocations during nanoindentation. *Physical Review B* 2003;**67**:172101–4.
10. Bradby JE, Williams JS, Swain MV. Pop-in events induced by spherical indentation in compound semiconductors. *Journal of Materials Research* 2004;**19**:380–6.
11. Page TF, Oliver WC, McHargue CJ. The deformation behavior of ceramic crystals subjected to very low load (nano)indentations. *Journal of Materials Research* 1992;**7**:450–73.
12. Kucheyev SO, Bradby JE, Williams JS, Jagadish C, Swain MV. Mechanical deformation of single-crystal ZnO. *Applied Physics Letters* 2002;**80**: 956–8.
13. Nowak R, Li CL, Swain MV. Comparison of implantation with Ni^{2+} and Au^{2+} ions on the indentation response of sapphire. *Materials Science and Engineering A-Structural Materials Properties Microstructure and Processing* 1998;**253**:167–77.
14. Wang XT, Padture NP. Shear strength of ceramics. *Journal of Materials Science* 2004;**39**:1891–3.
15. Tromas C, Colin J, Coupeau C, Girard JC, Woirgard J, Grilhe J. Pop-in phenomenon during nanoindentation in MgO. *European Physical Journal-Applied Physics* 1999;**8**:123–8.
16. Gaillard Y, Tromas C, Woirgard J. Pop-in phenomenon in MgO and LiF: observation of dislocation structures. *Philosophical Magazine Letters* 2003;**83**:553–61.
17. Minor AM, Morris JW, Stach EA. Quantitative in situ nanoindentation in an electron microscope. *Applied Physics Letters* 2001;**79**:1625–7.
18. Gouldstone A, Chollacoop N, Dao M, Li J, Minor AM, Shen YL. Indentation across size scales and disciplines: recent developments in experimentation and modeling. *Acta Materialia* 2007;**55**:4015–39.
19. Kelchner CL, Plimpton SJ, Hamilton JC. Dislocation nucleation and defect structure during surface indentation. *Physical Review B* 1998;**58**:11085–8.
20. Gouldstone A, Van Vliet KJ, Suresh S. Nanoindentation—simulation of defect nucleation in a crystal. *Nature* 2001;**411**:656–1656.
21. Kiely JD, Hwang RQ, Houston JE. Effect of surface steps on the plastic threshold in nanoindentation. *Physical Review Letters* 1998;**81**:4424–7.
22. Zimmerman JA, Kelchner CL, Klein PA, Hamilton JC, Foiles SM. Surface step effects on nanoindentation. *Physical Review Letters* 2001;**87**, 165507:1-4.
23. Bahr DF, Wilson DE, Crowson DA. Energy considerations regarding yield points during indentation. *Journal of Materials Research* 1999;**14**:2269–75.
24. Schuh CA, Lund AC. Application of nucleation theory to the rate dependence of incipient plasticity during nanoindentation. *Journal of Materials Research* 2004;**19**:2152–8.
25. Nowak R, Sekino T, Niihara K. Non-linear surface deformation of the $(10\bar{1}0)$ plane of sapphire: identification of the linear features around spherical impressions. *Acta Materialia* 1999;**47**:4329–38.
26. Vadalakonda S, Banerjee R, Puthcode A, Mirshams R. Comparison of incipient plasticity in bcc and fec metals studied using nanoindentation. *Materials Science and Engineering A-Structural Materials Properties Microstructure and Processing* 2006;**426**:208–13.
27. Nowak R, Chrobak D, Nagao S, Vodnick D, Berg M, Tukiainen A, Pessa M. An electric current spike linked to nanoscale plasticity. *Nature Nanotechnology* 2009;**4**:287–91.
28. Chrobak D, Nordlund K, Nowak R. Nondislocation origin of GaAs nanoindentation pop-in event. *Physical Review Letters* 2007;**98**, 045502:1-4.

29. Tymiak NI, Daugela A, Wyrobek TJ, Warren OL. Acoustic emission monitoring of the earliest stages of contact-induced plasticity in sapphire. *Acta Materialia* 2004;**52**:553–63.
30. Oliver WC, Pharr GM. Measurement of hardness and elastic modulus by instrumented indentation: advances in understanding and refinements to methodology. *Journal of Materials Research* 2004;**19**:3–20.
31. Bahr DF, Kramer DE, Gerberich WW. Non-linear deformation mechanisms during nanoindentation. *Acta Materialia* 1998;**46**:3605–17.
32. Lian J, Garay JE, Wang JL. Grain size and grain boundary effects on the mechanical behavior of fully stabilized zirconia investigated by nanoindentation. *Scripta Materialia* 2007;**56**:1095–8.
33. Tymiak NI, Gerberich WW. Initial stages of contact-induced plasticity in sapphire. II. Mechanisms of plasticity initiation. *Philosophical Magazine* 2007;**87**:5169–88.
34. Fischer-Cripps AC. *Nanoindentation*. New York: Springer; 2004. p. 3.
35. Bansal NP. *Handbook of ceramic composites*. Boston: Kluwer Academic Publishers; 2005. p. 211.
36. Martin M, Troyon M. Fundamental relations used in nanoindentation: critical examination based on experimental measurements. *Journal of Materials Research* 2002;**17**:2227–34.
37. Bei H, George EP, Hay JL, Pharr GM. Influence of indenter tip geometry on elastic deformation during nanoindentation. *Physical Review Letters* 2005:95.
38. Johnson KL. *Contact mechanics*. Cambridge: Cambridge University Press; 1985. p. 95.
39. Mitchell BS. *An introduction to materials engineering and science for chemical and materials engineers*. Chichester: John Wiley; 2004. p. 392.
40. Kelly A, Macmillan NH. *Strong solids*. Oxford: Clarendon; 1986. p. 395.
41. Okamoto NL, Kusakari M, Tanaka K, Inui H, Yamaguchi M, Otani S. Temperature dependence of thermal expansion and elastic constants of single crystals of ZrB_2 and the suitability of ZrB_2 as a substrate for GaN film. *Journal of Applied Physics* 2003;**93**:88–93.
42. Corcoran SG, Colton RJ, Lilleodden ET, Gerberich WW. Anomalous plastic deformation at surfaces: nanoindentation of gold single crystals. *Physical Review B* 1997;**55**:16057–60.
43. Ma L, Levine LE. Effect of the spherical indenter tip assumption on nanoindentation. *Journal of Materials Research* 2007;**22**:1656–61.
44. Krenn CR, Roundy D, Cohen ML, Chrzan DC, Morris JW. Connecting atomistic and experimental estimates of ideal strength. *Physical Review B* 2002;**65**:13411:1–13411:4.
45. Soer WA, Aifantis KE, De Hosson JTM. Incipient plasticity during nanoindentation at grain boundaries in body-centered cubic metals. *Acta Materialia* 2005;**53**:4665–76.
46. Asif SAS, Pethica JB. Nanoindentation creep of single-crystal tungsten and gallium arsenide. *Philosophical Magazine A-Physics of Condensed Matter Structure Defects and Mechanical Properties* 1997;**76**:1105–18.
47. Yang B, Vehoff H. Dependence of nanohardness upon indentation size and grain size—a local examination of the interaction between dislocations and grain boundaries. *Acta Materialia* 2007;**55**:849–56.
48. Shibutani Y, Koyama A. Surface roughness effects on the displacement bursts observed in nanoindentation. *Journal of Materials Research* 2004;**19**:183–8.
49. Basu S, Barsoum MW, Williams AD, Moustakas TD. Spherical nanoindentation and deformation mechanisms in freestanding GaN films. *Journal of Applied Physics* 2007;**101**, 083522:1-7.
50. Delafargue A, Ulm FJ. Explicit approximations of the indentation modulus of elastically orthotropic solids for conical indenters. *International Journal of Solids and Structures* 2004;**41**:7351–60.
51. Vlassak JJ, Nix WD. Measuring the elastic properties of anisotropic materials by means of indentation experiments. *Journal of the Mechanics and Physics of Solids* 1994;**42**:1223–45.
52. Berryman JG. Bounds and self-consistent estimates for elastic constants of random polycrystals with hexagonal, trigonal, and tetragonal symmetries. *Journal of the Mechanics and Physics of Solids* 2005;**53**:2141–73.
53. Thurn J, Morris DJ, Cook RF. Depth-sensing indentation at macroscopic dimensions. *Journal of Materials Research* 2002;**17**:2679–90.
54. Sakai M, Nakano Y. Elastoplastic load-depth hysteresis in pyramidal indentation. *Journal of Materials Research* 2002;**17**:2161–73.
55. Guicciardi S, Silvestroni L, Melandri C, Sciti D, Pezzotti G. Nanoindentation characterisation of HfC-based composites. *International Journal of Surface Science and Engineering* 2007;**1**:198–212.
56. Hay JC, Sun EY, Pharr GM, Becher PF, Alexander KB. Elastic anisotropy of beta-silicon nitride whiskers. *Journal of the American Ceramic Society* 1998;**81**:2661–9.
57. Vogelgesang R, Grimsditch M, Wallace JS. The elastic constants of single crystal β-Si_3N_4. *Applied Physics Letters* 2000;**76**:982–4.